

1 **Monitoring high-ozone events in the US Intermountain West using TEMPO**
2 **geostationary satellite observations**

3

4 Peter Zoogman^{1, †, *}, Daniel J. Jacob^{1,2}, Kelly Chance³, Xiong Liu³, Meiyun Lin⁴, Arlene Fiore⁵,
5 Katherine Travis²

6

7 1 Department of Earth and Planetary Sciences, Harvard University, Cambridge, MA, United
8 States

9 2 School of Engineering and Applied Sciences, Harvard University, Cambridge, MA, United
10 States

11 3 Harvard-Smithsonian Center for Astrophysics, Cambridge, MA, United States

12 4 Atmospheric and Ocean Sciences, Princeton University, Princeton, New Jersey, USA

13 5 Lamont-Doherty Earth Observatory, Columbia University, Palisades, NY, United States

14 † Present Address: Harvard-Smithsonian Center for Astrophysics, Cambridge, MA, United
15 States

16 *Corresponding Author. Tel: 9176129834. E-mail: pzoogman@cfa.harvard.edu. 60 Garden
17 Street, Cambridge, MA 02138

18 **Abstract**

19 High-ozone events, approaching or exceeding the National Ambient Air Quality Standard
20 (NAAQS), are frequently observed in the US Intermountain West in association with subsiding
21 air from the free troposphere. Monitoring and attribution of these events is problematic because
22 of the sparsity of the current network of surface measurements and lack of vertical information.
23 We present an Observing System Simulation Experiment (OSSE) to evaluate the ability of the
24 future geostationary satellite instrument Tropospheric Emissions: Monitoring of Pollution
25 (TEMPO), scheduled for launch in 2018-2019, to monitor and attribute high-ozone events in the
26 Intermountain West through data assimilation. TEMPO will observe ozone in the ultraviolet
27 (UV) and visible (Vis) to provide sensitivity in the lower troposphere. Our OSSE uses ozone data
28 from the GFDL AM3 chemistry-climate model (CCM) as the “true” atmosphere and samples it
29 for April-June 2010 with the current surface network (CASTNet sites), a configuration designed
30 to represent TEMPO, and a low Earth orbit (LEO) IR satellite instrument. These synthetic data
31 are then assimilated into the GEOS-Chem chemical transport model (CTM) using a Kalman
32 filter. Error correlation length scales (500 km in horizontal, 1.7 km in vertical) extend the range
33 of influence of observations. We show that assimilation of surface data alone does not
34 adequately detect high-ozone events in the Intermountain West. Assimilation of TEMPO data
35 greatly improves the monitoring capability, with little information added from the LEO
36 instrument. The vertical information from TEMPO further enables the attribution of NAAQS
37 exceedances to background ozone. This is illustrated with the case of a stratospheric intrusion.

38

39 **1. Introduction**

40 Harmful impacts of surface level ozone on both humans and vegetation is of increasing
41 concern in areas formerly considered remote. The US Environmental Protection Agency (EPA) is
42 considering lowering the current National Ambient Air Quality Standard (NAAQS) of 75 ppbv (parts
43 per billion by volume, fourth highest maximum daily 8-hour average per year) to a value in the range of
44 60-70 ppbv (EPA, 2012). Ozone concentrations in this range are frequently observed at high-elevation
45 sites in the western US with minimal local pollution influence (Lefohn et al., 2001). Although ozone
46 levels have been decreasing over the eastern US for the past two decades due to emissions controls,
47 there has been no such decrease in the West except for California (Cooper et al., 2012). Free
48 tropospheric ozone at 3-8 km altitude over the western US has been increasing by 0.41 ppbv
49 year⁻¹ during the past two decades (Cooper et al., 2012), which could affect background surface
50 concentrations in the West (Zhang et al., 2008). There has been great interest in using satellite
51 observations of ozone and related species to monitor and attribute background surface ozone
52 (Lin et al., 2012a; Fu et al., 2013). This capability has been limited so far by the temporal
53 sparseness of satellite data and low sensitivity to the surface. All satellite measurements so far
54 have been from low Earth orbit (LEO). Here we show that multispectral measurements from a
55 configuration designed to represent the best current estimate of the NASA Tropospheric
56 Emissions: Monitoring of Pollution (TEMPO) geostationary satellite mission over North America,
57 scheduled for launch in 2018-2019, can provide a powerful ozone monitoring resource to
58 complement surface sites, and can help to identify NAAQS exceedances caused by elevated
59 background.

60 The North American background is defined by the EPA as the surface ozone concentration
61 that would be present over the US in the absence of North American anthropogenic emissions. It

62 includes natural sources and intercontinental pollution, and represents a floor for the achievable
63 benefits from domestic emissions control policies (including agreements with Canada and
64 Mexico). The North American background is particularly high in the Intermountain West, a
65 region extending between the Sierra Nevada/Cascades on the west and the Rocky Mountains on
66 the east, due to high elevation and arid terrain (Zhang et al., 2011). Subsidence of high-ozone air
67 from the free troposphere can cause surface ozone concentrations in that region to approach or exceed
68 the NAAQS (Reid et al., 2008). This is not an issue in the eastern US because of lower elevation,
69 forest cover, and high moisture (Fiore et al., 2002).

70 Background effects on surface ozone air quality are important to diagnose, as NAAQS
71 exceedances can be dismissed as exceptional events if shown to be not reasonably controllable
72 by local governances (EPA 2013). Monitoring of ozone in the Intermountain West is mostly
73 performed at urban stations designed to observe local pollution and not background influences.
74 There is a limited network of Clean Air Status and Trends Network (CASTNet;
75 www.epa.gov/castnet) sites located at national parks and other remote locations, and these have
76 been used extensively to estimate background ozone and evaluate models (Fiore et al., 2002;
77 Zhang et al., 2011; Lin et al., 2012b; Cooper et al., 2012). Langford et al. (2009) demonstrated
78 that transport of stratospheric air contributed to surface one-minute average ozone concentrations
79 in excess of 100 ppbv in Colorado in 1999. Analysis of ozonesonde and lidar measurements by
80 Lin et al [2012b] indicates thirteen stratospheric intrusions in spring 2010 leading to observed
81 maximum daily 8-hour average (MDA8) ozone of 70-86 ppbv at surface sites. Yates et al. (2013)
82 similarly demonstrated a stratospheric origin for a NAAQS exceedance in Wyoming in June
83 2012 by using a combination of 3-D modeling, aircraft observations, LEO satellite data, and
84 geostationary weather satellites. But the current air quality observing system is very limited in
85 its ability to (1) monitor ozone at sites prone to high background, and (2) diagnose the origin of
86 high-ozone events at these sites.

87 Several chemical transport models (CTMs) and one chemistry-climate model (CCM)
88 have been used to estimate the North American background including GEOS-Chem (Fiore et al.,
89 2003; Zhang et al., 2011), GFDL AM3 CCM (Lin et al., 2012a,b), CMAQ (Mueller and Mallard
90 2011), and CAMx (Emery et al., 2012). Values average 30-50 ppbv in spring and summer over
91 the Intermountain West with events exceeding 60 ppbv. There are large differences between
92 models reflecting variable contributions from the stratosphere (Lin et al. 2012b), lightning
93 (Kaynak et al. 2008, Zhang et al. 2011), and wildfires (Mueller and Mallard, 2011; Zhang et al.,
94 2011; Jaffe and Wigder, 2012; Singh et al., 2012).

95 Geostationary satellites are a promising tool to address the limitations of the current observing
96 system (Fishman et al., 2012; Lahoz et al., 2012). These satellites orbit the Earth with a 24-h period in
97 an equatorial plane, thus continuously staring at the same scenes. Depending on the observing strategy,
98 they may provide hourly ozone data over a continental domain, while a LEO satellite may offer at best
99 a 1-day return time. A global constellation of geostationary satellite missions targeted at air quality is
100 planned to launch in 2018-2019 including TEMPO over North America (Chance et al. 2012),
101 SENTINEL-4 over Europe (Ingmann et al., 2012), and GEMS over East Asia (Kim 2012; Bak et al.,
102 2013).

103 TEMPO will measure backscattered solar radiation in the 290-740 nm range, including
104 the ultraviolet (UV) and visible Chappuis (Vis) ozone bands (Chance et al., 1997; Liu et al.,
105 2005). Sentinel-4 and GEMS will only measure ozone in the UV. Observation in the weak
106 Chappuis band takes advantage of the relative transparency of the atmosphere in the Vis to

107 achieve sensitivity to near-surface ozone (Natraj et al., 2011; Selitto et al., 2012a). An observing
108 system simulation experiment (OSSE) by Zoogman et al. (2011) shows that a UV+Vis instrument in
109 geostationary orbit could provide useful constraints on surface ozone through data assimilation.

110 Here we conduct an OSSE to quantify the potential of geostationary ozone measurements
111 from TEMPO to improve monitoring of ozone NAAQS exceedances in the Intermountain West
112 and the role of background ozone in causing these exceedances. Our goal is to inform the TEMPO
113 observing strategy and develop methods for exploitation of TEMPO data. OSSEs have previously
114 informed mission planning for geostationary observations of atmospheric composition (Edwards et al.,
115 2009; Timmermans et al., 2009; Claeys et al., 2011; Zoogman et al., 2011, 2014; Selitto et al.,
116 2014). An important feature of our work here is the inclusion of surface network and LEO
117 satellite observations in the data assimilation system to properly quantify the added benefit of
118 TEMPO observations.

119 Section 2 outlines the OSSE framework including a description and comparison of the
120 simulation models used, the present and future observing systems considered, the data
121 assimilation system, and the quantification of the error correlation length scales. Section 3
122 describes the OSSE results showing improved monitoring of surface ozone across the
123 Intermountain West from TEMPO observations and improved detection of high-ozone events in
124 the Intermountain West by data assimilation. Section 4 presents a case study of a stratospheric
125 intrusion demonstrating the detection of an exceptional ozone event by TEMPO its attribution to
126 the North American background. Section 5 summarizes the results and discusses future research
127 directions.

128 **2. Observing System Simulation Experiment (OSSE)**

129 OSSEs are a standard technique for assessing the information to be gained by data assimilation
130 from adding a new instrument to an existing observing system (Lord et al., 1997). The OSSE
131 framework involves the use of a model to generate synthetic time-varying 3-D fields of concentrations
132 (taken as the “true” atmosphere), and the virtual sampling of this “true” atmosphere by the different
133 instruments composing the observing system for data assimilation. This virtual sampling follows the
134 observing schedules and error characteristics of each instrument. The virtual observations are then
135 assimilated in a second, preferably independent model, and the results of the assimilation (with and
136 without the new instrument) are compared to the “true” atmosphere to assess the value of the new
137 instrument (Edwards et al., 2009).

138 We conduct our OSSE for April-June 2010, corresponding to the seasonal maximum in
139 background ozone over the Intermountain West (Brodin et al., 2010). The observing system includes
140 the CASTNet surface network, a LEO instrument, and TEMPO. The LEO and TEMPO instruments in
141 this study represent the best current estimate of future instrument characteristics. The “true”
142 atmosphere is provided by the GFDL AM3 CCM (Lin et al., 2012a,b). The model used for data
143 assimilation (“forward model”) is the GEOS-Chem CTM (Zhang et al, 2011); it generates *a priori*
144 concentrations at successive time steps to be corrected to the “true” atmosphere by the observing
145 system through data assimilation. The information provided by the observing system is quantified by
146 the correction of the mismatch between the “true” state and the *a priori*. We describe below our OSSE
147 framework including the simulation models (GFDL AM3 and GEOS-Chem), the observing system,
148 and the data assimilation system.

149 2.1 Simulation Models

150 We use for our “true” atmosphere the GFDL AM3 global chemistry-climate model with
151 horizontal resolution of $1/2^\circ \times 5/8^\circ$ (latitude x longitude) nudged to reanalysis winds (Lin et al.,
152 2012a,b). This CCM was successful in reproducing background ozone variability and exceptional
153 events in the Western US during the CalNex field campaign in April-June 2010 (Lin et al., 2012b).
154 This is important because the “true” model should reproduce the characteristics of the
155 observations relevant to the OSSE. Lin et al. (2012a,b) used GFDL AM3 to investigate the effect of
156 Asian transport and stratospheric intrusions on surface ozone in the Intermountain West during April-
157 June 2010, and they quantified the ozone background through a sensitivity simulation with North
158 American anthropogenic sources shut off. Here we use 3-hourly concentrations archived from
159 their standard simulation to provide the global 3-D ozone fields of the “true” atmosphere.

160 Our forward model for data assimilation is the GEOS-Chem CTM (Bey et al., 2001;
161 <http://www.geos-chem.org>) driven by GEOS assimilated meteorological data from the NASA Global
162 Modeling and Assimilation Office (GMAO). The GEOS-Chem version used here (v8-02-03) was
163 previously described by Zhang et al. (2011) in a study of background ozone influence on the
164 Intermountain West during 2006-2008. It covers the North America domain with $1/2^\circ \times 2/3^\circ$
165 horizontal resolution ($10^\circ\text{N} - 60^\circ\text{N}$, $140^\circ\text{W} - 40^\circ\text{W}$), nested within a global domain with $2^\circ \times 2.5^\circ$
166 horizontal resolution. GEOS-Chem and GFDL AM3 have completely separate development heritages
167 and use different driving meteorological fields, chemical mechanisms, and emission inventories. This
168 independence between the two models used in the OSSE is important for a rigorous assessment
169 (Arnold and Dey 1986). The horizontal resolution of both models (~50 km) is adequate for
170 characterization of background ozone.

171 **Figure 1** shows the maximum daily average 8-hour (MDA8) ozone concentrations in surface
172 air for each model, averaged over April-June 2010. GFDL AM3 has higher ozone concentrations than
173 GEOS-Chem over the US as a whole and over the Intermountain West (bordered region) in particular.
174 Zhang et al. (2011) previously showed that GEOS-Chem can reproduce ozone concentrations in
175 the Intermountain West up to 70 ppbv with relatively little error, but cannot reproduce
176 exceptional events of higher concentrations. GFDL AM3 has a high mean bias but better
177 simulates high-ozone events than GEOS-Chem (Lin et al., 2012b).

178

179 2.2 Observing System and Synthetic Observations

180 Our OSSE simulates the anticipated ozone observing system over the Intermountain West
181 during operation of TEMPO. This will consist of surface measurements, LEO satellite
182 measurements, and TEMPO geostationary satellite measurements. As the LEO and TEMPO
183 instruments are still in mission planning, assumptions must be made for their final
184 characteristics. For the LEO satellite measurements we assume a future version of the Infrared
185 Atmospheric Sounding Interferometer (IASI) instrument, IASI-3, that will be launched in 2016 on the
186 MetOp-C satellite (Clerbaux, 2009). IASI retrieves ozone in the thermal infrared (TIR). We also expect
187 to have in that time frame UV ozone observations from the Tropospheric Monitoring Instrument
188 (TROPOMI), scheduled for LEO launch in 2015 (<http://www.tropomi.eu>). TIR and UV ozone
189 instruments have similar vertical sensitivities (Zhang et al., 2010). TIR has the advantage of providing
190 observations at night that will be complementary to the TEMPO mission.

191 CASTNet provides hourly data for 12 surface sites in the Intermountain West (Figure 1)
192 that are used for background monitoring (EPA, 2013). Although these sites are sparse, they are
193 intended to be regionally representative and exhibit significant spatial correlation (Jaffe, 2011).
194 CASTNet stations outside of the Intermountain West are not used; we assumed they do not
195 provide useful constraints for the region but it is possible certain California sites might be
196 exceptions. CASTNet ozone measurements have 2% instrument error (EPA, 2010). There is
197 additional representation error when assimilating CASTNet data into a model due to the spatial
198 mismatch between the point where the measurement is taken and the model gridsquare mean to
199 which it is compared. We find a representation error of 5% for the $\sim 50 \times 50 \text{ km}^2$ gridsquare size of
200 GEOS-Chem, based on the model error correlation length scale (see Section 2.4). During
201 nighttime the representation error could be much larger due to surface air stratification. Thus we
202 only assimilate CASTNet data during daytime.

203 TEMPO and IASI-3 will both be nadir viewing satellite instruments, with retrieval of
204 vertical concentration profiles to be made by optimal estimation (Rodgers, 2000). If \mathbf{x}_p is the true
205 profile, i.e. the vector of true concentrations in an observation column, then the retrieved profile
206 \mathbf{x}_p' is related to \mathbf{x}_p by the instrument averaging kernel matrix \mathbf{A} which defines the sensitivity of
207 \mathbf{x}_p' to \mathbf{x}_p ($\mathbf{A} = \partial \mathbf{x}_p' / \partial \mathbf{x}_p$):

$$208 \quad \mathbf{x}_p' = \mathbf{x}_s + \mathbf{A}(\mathbf{x}_p - \mathbf{x}_s) + \boldsymbol{\varepsilon} \quad (1)$$

209 where $\boldsymbol{\varepsilon}$ is the instrument noise vector and \mathbf{x}_s is an independent *a priori* ozone profile used to
210 regularize the retrieval.

211 **Figure 2** shows typical clear-sky averaging kernel matrices for UV+Vis and TIR retrievals of
212 tropospheric ozone taken from the Natraj et al. (2011) theoretical study. Also shown are the degrees
213 of freedom for signal (DOFS) below given pressure levels. The DOFS are the number of independent
214 pieces of information in the vertical provided by the retrieval, as determined from the corresponding
215 trace of the averaging kernel matrix. The profile (index 5 from Natraj et al. 2011) used to generate
216 these averaging kernels has moderate ozone (58 ppbv), moderate temperature contrast, and an
217 intermediate viewing geometry, making it consistent with conditions in the Intermountain West.
218 The assumed Vis surface albedo may be lower than the actual albedo which would result in an
219 underestimation of TEMPO sensitivity to near-surface ozone. The UV+Vis spectral ranges (290-
220 340 nm, 560-620 nm) and spectral resolution (0.4 nm) assumed by Natraj et al. (2011) are
221 comparable to the spectral ranges (290-490 nm, 540-740 nm) and spectral resolution (0.6 nm)
222 planned for TEMPO. The TEMPO instrument is still under development and thus does not have
223 its characteristics fully finalized; Natraj et al. (2011) gives the published best estimate of
224 TEMPO ozone sensitivities. We expect TEMPO ozone sensitivities to be similar to UV+Vis
225 sensitivities from Natraj et al. (2011). The additional near-surface information provided by the
226 UV+Vis combination is consistent with previous work using SCIAMACHY data (Selitto et al.,
227 2012b).

228 We generate synthetic geostationary observations from the GFDL AM3 “true”
229 atmosphere by sampling daytime vertical profiles over land in the North American domain with
230 the averaging kernel matrix given in Figure 2. Acknowledging that the actual configuration of
231 TEMPO is still under development, we henceforth refer to these synthetic geostationary
232 observations as TEMPO. TEMPO observations over the ocean are not included as the planned field
233 of regard for the mission includes very little ocean and because the clear ocean surface is too dark for

234 Vis retrievals. We similarly generate synthetic LEO IASI-3 (henceforth LEO) observations over the
 235 North American domain twice a day (local noon and midnight) with the averaging kernel matrix given
 236 in **Figure 2**. These TIR measurements are intended as representative of ozone observations from
 237 LEO instruments operational during the TEMPO lifetime. We omit scenes with cloud fraction > 0.3
 238 (as given by the GEOS meteorological data). We assume fixed averaging kernel matrices,
 239 acknowledging that in practice there is significant variability (Worden et al., 2013). Gaussian
 240 noise is added to the synthetic observations following Natraj et al. (2011) to simulate the random error
 241 associated with the spectral measurement. The noise from the TEMPO instrument (footprint of 4×8
 242 km^2) is reduced by the square root of the number of observations averaged over each GEOS-Chem grid
 243 square ($\sim 50 \times 50 \text{ km}^2$) in the data assimilation process. Since the TEMPO measurements are spatially
 244 dense we assume zero representation error during assimilation. Current IASI measurements have
 245 footprint diameters of 12-40 km with centers spaced 25-80 km apart (August et al., 2012); no reduction
 246 of the random error is applied to the LEO observations.

247 **2.3 Assimilation of surface and satellite measurements**

248 The goal of our data assimilation system is to optimize an n -element state vector (\mathbf{x}) of 3-
 249 D tropospheric ozone concentrations over the North American domain of GEOS-Chem, using
 250 surface and satellite observations to correct the GEOS-Chem simulation at successive time steps.
 251 CASTNet and TEMPO data are assimilated at discrete 3-h time steps, and LEO data are
 252 assimilated at 12-h time steps. We use a Kalman filter, as previously applied to ozone data
 253 assimilation by Khattatov et al (2000), Parrington et al. (2008), and Zoogman et al. (2011). At
 254 each time step, we calculate an optimal estimate $\hat{\mathbf{x}}$ of the true ozone concentrations \mathbf{x} as a weighted
 255 average of the model forecast \mathbf{x}_a (with corresponding error vector $\boldsymbol{\varepsilon}_a$ relative to the true concentrations)
 256 and the observations \mathbf{x}' (with observational error $\boldsymbol{\varepsilon}'$ and with \mathbf{x}' set to \mathbf{x}_a where there are no
 257 observations). The observational error includes both the instrument noise $\boldsymbol{\varepsilon}$ and (for surface sites) the
 258 previously defined representation error. The errors are characterized by error covariance matrices $\mathbf{S}_a =$
 259 $E[\boldsymbol{\varepsilon}_a \boldsymbol{\varepsilon}_a^T]$ and $\mathbf{S}_\varepsilon = E[\boldsymbol{\varepsilon}' \boldsymbol{\varepsilon}'^T]$, where $E[\]$ is the expected-value operator. Assuming Gaussian error
 260 distributions for $\boldsymbol{\varepsilon}_a$ and $\boldsymbol{\varepsilon}$ we obtain (Rodgers, 2000):

$$261 \quad \hat{\mathbf{x}} = \mathbf{x}_a + \mathbf{G}(\mathbf{x}' - \mathbf{K}\mathbf{x}_a) \quad (2)$$

262 where \mathbf{K} is the observation operator that maps the model forecast to the observations. For satellite
 263 measurements $\mathbf{K}\mathbf{x}_a = \mathbf{x}_s + \mathbf{A}(\mathbf{x}_a - \mathbf{x}_s)$ (equation (1) with no noise term), while for surface measurements
 264 $\mathbf{K}\mathbf{x}_a = \mathbf{x}_a$. The gain matrix \mathbf{G} is given by

$$265 \quad \mathbf{G} = \mathbf{S}_a \mathbf{K}^T (\mathbf{K} \mathbf{S}_a \mathbf{K}^T + \mathbf{S}_\varepsilon)^{-1} \quad (3)$$

266 and determines the relative weight given to the observations and the model. The instrument error
 267 covariance matrix \mathbf{S}_ε is assumed diagonal and set to an arbitrarily large number in locations
 268 where there are no observations. For surface measurements we include the 5% representation
 269 error in quadrature with the 2% instrument error so that the corresponding error variances are
 270 additive. The optimal estimate $\hat{\mathbf{x}}$ has error $\hat{\boldsymbol{\varepsilon}}$ with error covariance $\hat{\mathbf{S}} = E[\hat{\boldsymbol{\varepsilon}} \hat{\boldsymbol{\varepsilon}}^T]$:

$$271 \quad \hat{\mathbf{S}} = (\mathbf{I}_n - \mathbf{G}\mathbf{K})\mathbf{S}_a \quad (4)$$

272 Where \mathbf{I}_n is the identity matrix of dimension n .

273 The model error covariance matrix \mathbf{S}_a expresses the error in the forward model at each
274 assimilation time step and is given by:

$$275 \quad \mathbf{S}_a = \begin{pmatrix} \text{var}(\boldsymbol{\varepsilon}_{a,1}) & \cdots & \text{cov}(\boldsymbol{\varepsilon}_{a,1}, \boldsymbol{\varepsilon}_{a,n}) \\ \vdots & \ddots & \vdots \\ \text{cov}(\boldsymbol{\varepsilon}_{a,n}, \boldsymbol{\varepsilon}_{a,1}) & \cdots & \text{var}(\boldsymbol{\varepsilon}_{a,n}) \end{pmatrix} \quad (5)$$

276 where $\boldsymbol{\varepsilon}_a = (\boldsymbol{\varepsilon}_{a,1}, \dots, \boldsymbol{\varepsilon}_{a,n})^T$, with $\boldsymbol{\varepsilon}_{a,i}$ representing the error for GEOS-Chem gridbox i . Following
277 Zoogman et al. (2011), we initialize \mathbf{S}_a at the beginning of the simulation as a diagonal matrix
278 with *a priori* errors of 29% (quantified by comparison of GEOS-Chem to ozonesonde
279 measurements), and update it at each assimilation time step on the basis of the computed *a*
280 *posteriori* error covariance matrix $\hat{\mathbf{S}}$ (equation (4)). The diagonal terms of $\hat{\mathbf{S}}$ are transported as
281 tracers in GEOS-Chem to the next assimilation time step and are augmented by a model error variance
282 reflecting the time-dependent divergence of the model from the true state (Zoogman et al., 2011). This
283 yields the diagonal terms $\text{var}(\boldsymbol{\varepsilon}_{a,i})$ of \mathbf{S}_a for the next assimilation time step. The off-diagonal
284 terms (error covariances) describe the propagation of information from each observation over a
285 spatial domain of influence. We compute $\text{cov}(\boldsymbol{\varepsilon}_{a,i}, \boldsymbol{\varepsilon}_{a,j})$ for each pair of gridboxes (i,j) as a
286 function of the horizontal and vertical distance between the two gridboxes using the error
287 correlation length scales from section 2.4.

288 In practice the dimension of the matrices used in the assimilation must be limited to make
289 the computation tractable. This is done by solving Eq. (2) column by column and including only
290 measurements at a horizontal distance less than 510 km (the horizontal error correlation length
291 scale, see below) in the model error covariance matrix.

292

293 2.4 Error Correlation Length Scales

294 The spatial extent of information provided by an observation to correct the GEOS-Chem
295 model simulation through data assimilation can be quantified by correlating the GEOS-Chem
296 errors relative to *in situ* observations at different sites in the Intermountain West (for the
297 horizontal scale) and ozonesonde profiles (for the vertical scale). To define a horizontal error
298 correlation length scale we used actual CASTNet surface measurements from our period of study
299 (April-June 2010), downloaded from <http://epa.gov/castnet/>. We compute the time series of
300 model error during daytime (0900 – 1700 LT) at each surface site, and from there derive the
301 model error correlation between each pair of surface sites. **Figure 3 (left)** shows the correlation
302 coefficients plotted against the distance d between sites (binned every 100km). We find $R = \exp(-$
303 $d/510 \text{ km})$. We also show the error correlation length scale calculated when comparing GEOS-
304 Chem and GFDL AM3 (in red) sampled over the Intermountain West region. The model-model
305 error correlation length scale is similar to the model-observation length scale, providing support
306 for the realism of error patterns in our OSSE. We assume that the horizontal error correlation
307 length scale is invariant with altitude.

308 To estimate the vertical correlation length scale we compare GEOS-Chem ozone
309 concentrations to *in situ* vertical profiles from May-June 2010 ozonesondes at six locations in

310 California (Cooper et al. 2011). **Figure 3 (right)** shows the correlation coefficients plotted
311 against the vertical distance z (binned every 500 m) for the time series of model errors at each
312 ozonesonde station from the surface to 8 km altitude. We find $R = \exp(-z/1.7 \text{ km})$. Again, the
313 model-model length scale (red) is not significantly different from the model-observation length
314 scale.

315

316 **3. TEMPO observation of high-ozone events in the Intermountain West**

317 We now apply our OSSE system to evaluate the benefit of TEMPO observations to
318 monitor and attribute ozone exceedances in the Intermountain West. We compare the “true”
319 concentrations in surface air over the Intermountain West to GEOS-Chem CTM ozone
320 concentrations without data assimilation (*a priori*) and with assimilation of synthetic CASTNet,
321 TEMPO, and IASI-3 LEO observations. We also performed an assimilation of CASTNet and
322 TEMPO observations without a LEO instrument and found no significant difference in results.
323 Thus the LEO instrument does not add significant information beyond TEMPO for constraining
324 surface ozone concentrations in the Intermountain West. Its value for tracking exceptional events
325 will be discussed in section 4.

326 **Figure 4** examines the ability of the data assimilation system to monitor daily MDA8
327 ozone over the Intermountain West at the $1/2^\circ \times 2/3^\circ$ ($\sim 50 \times 50 \text{ km}^2$) GEOS-Chem grid resolution.
328 The top panel shows a scatterplot of *a priori* GEOS-Chem MDA8 ozone concentrations in April-
329 June 2010, for individual grid squares over the Intermountain West domain of Figure 1 and
330 individual days, vs. the “true” concentrations from the GFDL AM3 model. The GEOS-Chem *a*
331 *priori* is biased low and performs poorly in reproducing the “true” variability ($R^2=0.12$, bias = -
332 9.0 ppbv). Assimilation of synthetic CASTNet surface measurements reduces the low bias from
333 9.0 to 2.8 ppbv, but still does not capture much of the variability ($R^2=0.34$). Adding the synthetic
334 TEMPO geostationary observations eliminates the low bias and captures over half of the
335 variability ($R^2=0.58$).

336 The ability of TEMPO observations to capture high-ozone events is of particular interest.
337 **Figure 5** shows a map of the number of days in April-June 2010 with MDA8 ozone in excess of
338 70 ppbv for individual GEOS-Chem gridsquares in the Intermountain West. Values are shown
339 for the “true” atmosphere, the GEOS-Chem *a priori* without data assimilation, and the data
340 assimilation results including only the CASTNet observations and with the addition of TEMPO
341 observations. The “truth” shows an average of 5.7 high-ozone events per gridsquare in the
342 Intermountain West over the April-June 2010 period. The *a priori* model has only 0.8 event-days
343 per gridsquare and the spatial pattern is very different (spatial correlation $R^2=0.09$ for the
344 ensemble of Intermountain West gridsquares). Assimilation of surface measurements improves
345 both the average number of high-ozone events (3.6 event-days) and the spatial pattern ($R^2=0.62$).
346 The inability to fully correct the bias is due in part to the large impact of free tropospheric air in
347 driving high-ozone events, and in part to the limited coverage from the sparse surface network.
348 Adding TEMPO satellite observations almost fully corrects the bias (mean of 5.4 event-days)
349 and captures most of the spatial distribution of high-ozone events ($R^2=0.82$).

350

351 **4. Attribution of exceptional events using TEMPO observations**

352 TEMPO will provide continuous daytime observation in the free troposphere as well as in
353 the boundary layer, with separation between the two (Figure 2). Thus it could be particularly

354 powerful in quantifying free tropospheric background contributions to NAAQS exceedances.
355 This would assist in the designation of exceptional events where an exceedance of the NAAQS is
356 considered to be outside local control.

357 We examine a case study of a stratospheric intrusion on June 13 in the GFDL AM3
358 model taken as the “truth”. **Figure 6** shows a time series for June 2010 of MDA8 ozone
359 concentrations at a location in northern New Mexico (107°W, 36°N). We choose this event as it
360 was diagnosed by ozonesonde observations and meteorological tracers as a deep stratospheric
361 intrusion event (Lin et al., 2012a). Actual observations at nearby CASTNet locations indicate
362 ozone in excess of 75 ppbv during this modeled intrusion.

363 Evidence of free tropospheric origin for the June 13 event is critical to achieving an
364 “exceptional event” designation. **Figure 7** (top left) shows a longitude-altitude cross section of
365 ozone concentrations in the GFDL AM3 model taken as the “truth”. The stratospheric intrusion
366 is manifest at 103-109°W. The *a priori* GEOS-Chem model (top right) also shows a stratospheric
367 ozone enhancement extending to the surface but of much smaller magnitude. Assimilation of
368 surface measurements (not shown) makes little correction in the free troposphere. Synthetic
369 satellite measurement imagery from TEMPO without assimilation (bottom left) shows elevated
370 values in the free troposphere but does not properly represent surface gradients due to instrument
371 smoothing. Assimilating TEMPO observations into the GEOS-Chem CTM together with LEO
372 measurements (bottom right) captures the magnitude and spatial structure of the stratospheric
373 intrusion, and this would make a strong case for diagnosis of an exceptional event. We see here
374 that the use of data assimilation efficiently enhances the information from TEMPO to constrain
375 surface air concentrations. Information from the LEO instrument does not add significantly in
376 this case to observations from TEMPO, although it does correct ozone fields over the ocean
377 where TEMPO does not observe in this OSSE. The LEO instrument will thus be valuable for
378 tracking transpacific transport of ozone plumes even when TEMPO is operational.

379 380 **5. Summary**

381 We demonstrated the potential of future TEMPO UV+Vis geostationary observations to
382 monitor ozone exceedances in the Intermountain West and identify those exceedances caused by
383 the North American background. Our goal was to inform the TEMPO observing strategy and
384 develop methods for exploitation of its data. To accomplish this we performed an observation system
385 simulation experiment (OSSE) for assimilation of synthetic TEMPO data designed to best represent
386 future observations based on current estimates of TEMPO instrument characteristics. We used
387 two global 3-D ozone models with ~50 km horizontal resolution, one as the “true” atmosphere and one
388 as the forward model for data assimilation. We also included in our OSSE surface measurements from
389 the current CASTNet monitoring network sites in the Intermountain West (12 sites) and satellite
390 measurements from a thermal infrared (TIR) low Earth orbit (LEO) instrument projected to be in orbit
391 concurrently with TEMPO.

392 An important factor in data assimilation is the scales over which observed information
393 can be propagated with the forward model. We quantified this using model error correlation
394 length scales for the Intermountain West based on actual CASTNet and ozonesonde data. We
395 find length scales of 500 km (horizontal) and 1.7 km (vertical). These are in close agreement
396 with error correlation length scales between the two models used in our OSSE.

397 We find that the CASTNet surface observations are too sparse to adequately monitor
398 high-ozone events in the Intermountain West even after data assimilation. We show that the
399 TEMPO geostationary observations will provide a greatly improved observing system for

400 monitoring such events, eliminating the *a priori* model bias, capturing 58% of surface MDA8
401 ozone variability, and capturing 82% of the distribution of high-ozone days. In addition, because
402 of the information they provide on the vertical distribution of ozone, they can effectively
403 diagnose NAAQS exceedances caused by background ozone. Our evidence indicates that a LEO
404 satellite instrument flying concurrently with TEMPO provides no significant added value for
405 monitoring the ozone background over the US but could be useful for tracking transpacific
406 plumes.

407 The use of invariant averaging kernel matrices is a limitation of this study. Preparation
408 for TEMPO must include improved constraints on physical parameters, such as surface albedo,
409 that can vary greatly over the North American domain and that affect the sensitivity of UV+Vis
410 retrievals of near-surface ozone. Also, if the differences between the two models used in our
411 OSSE are larger than future errors in modeled ozone, this study may overestimate the
412 information TEMPO will provide. However, our OSSE demonstrates the large relative
413 improvement of information provided by TEMPO over the current observing system.

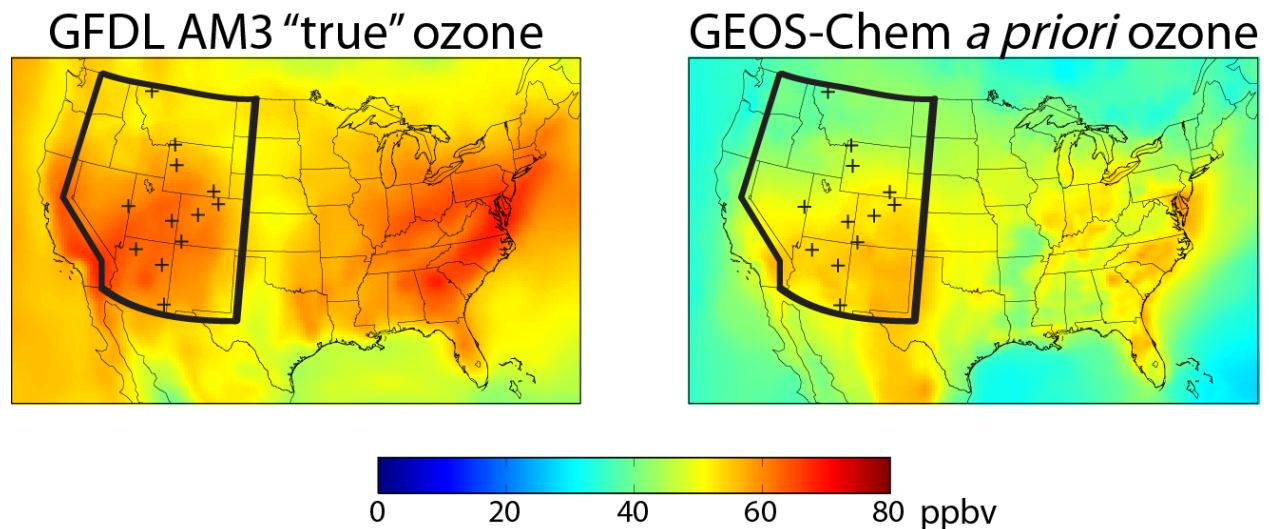
414 Use of the complete observing system described here (surface, geostationary, and LEO)
415 will provide a powerful tool for future air quality policy. Planning is underway to combine this
416 system with regional air quality models to supply the public with near real time pollution reports
417 and forecasts. These reports and forecasts would be much the same as currently available
418 weather information, also provided in large part from geostationary satellite observations.

419

420 **Acknowledgements:** This work was supported by the NASA Earth Science Division and by a NASA
421 Earth and Space Science Fellowship to Peter Zoogman.

422

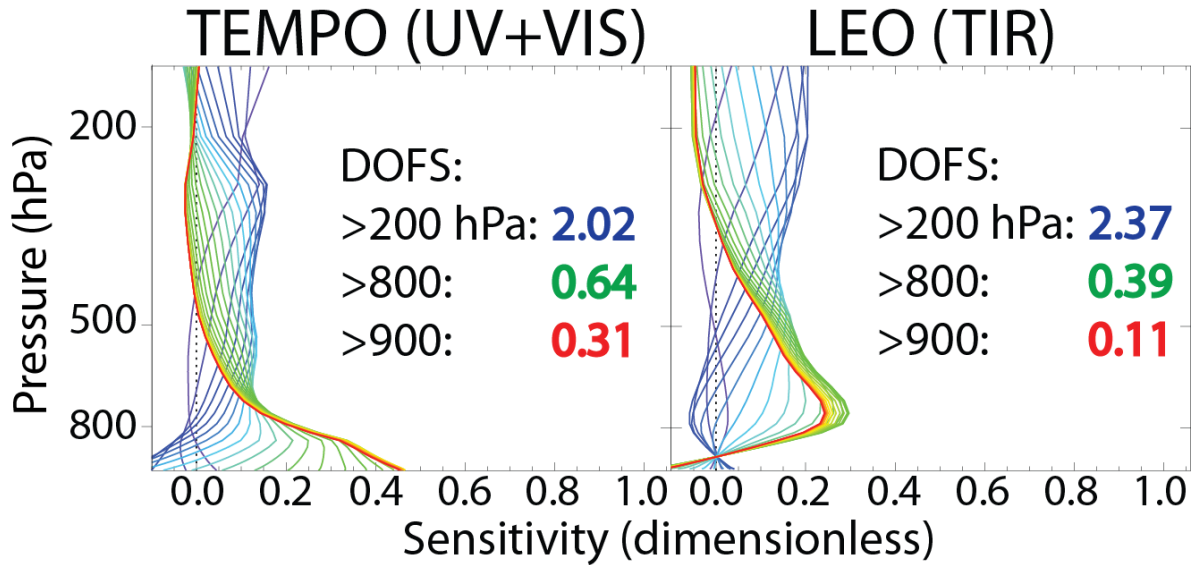
423 **Figures:**



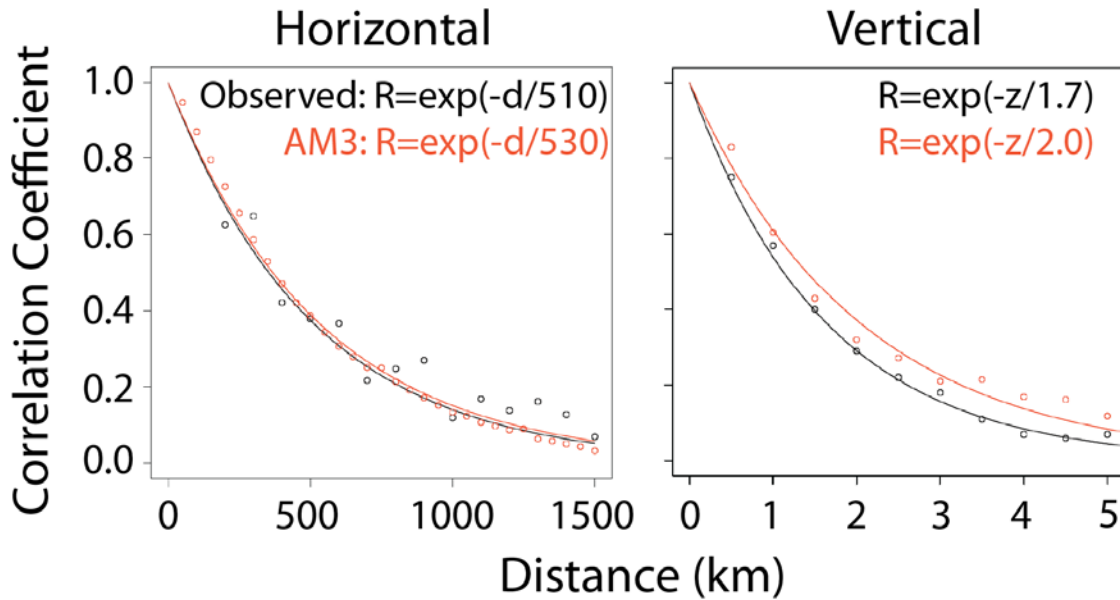
424

425 **Figure 1:** Mean values of the daily maximum 8-hour average (MDA8) ozone concentrations for
426 April-June 2010 in surface air. Left panel shows values from the GFDL AM3 CCM used as the

427 “true” atmosphere in our OSSE. Right panel shows the *a priori* values from the GEOS-Chem
 428 CTM used for data assimilation. Red/blue coloring denotes relatively high/low ozone values
 429 respectively. The black lines delineate the Intermountain West and black crosses show CASTNet
 430 surface measurement sites in the region.

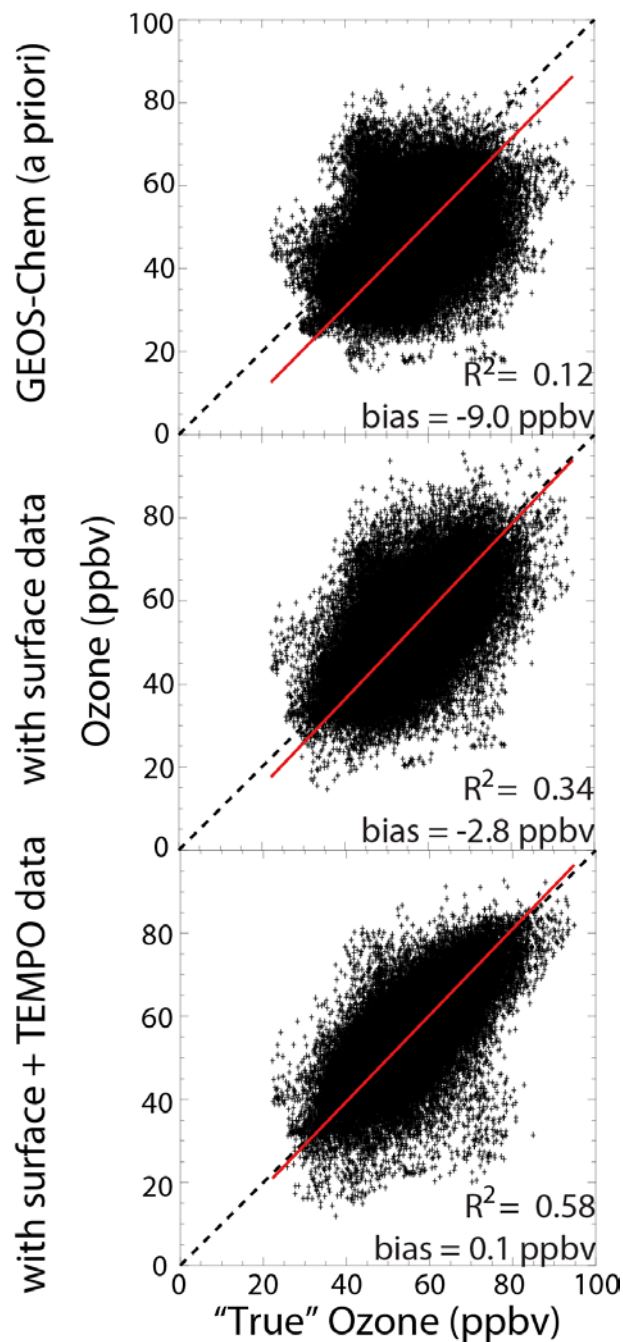


431
 432 **Figure 2:** Normalized averaging kernel matrices assumed in this study (from Natraj et al. [2011])
 433 for clear-sky retrievals of tropospheric ozone from space in the UV+Vis (left) and the TIR
 434 (right). UV+Vis in our study corresponds to TEMPO, while TIR corresponds to a future LEO
 435 instrument flying concurrently with TEMPO. Lines are matrix rows for individual vertical levels,
 436 with the color gradient from red to blue corresponding to vertical levels ranging from surface air (red)
 437 to 200 hPa (blue). Inset are the degrees of freedom for signal (DOFS) for the atmospheric columns
 438 below 200, 800, and 900 hPa.



439

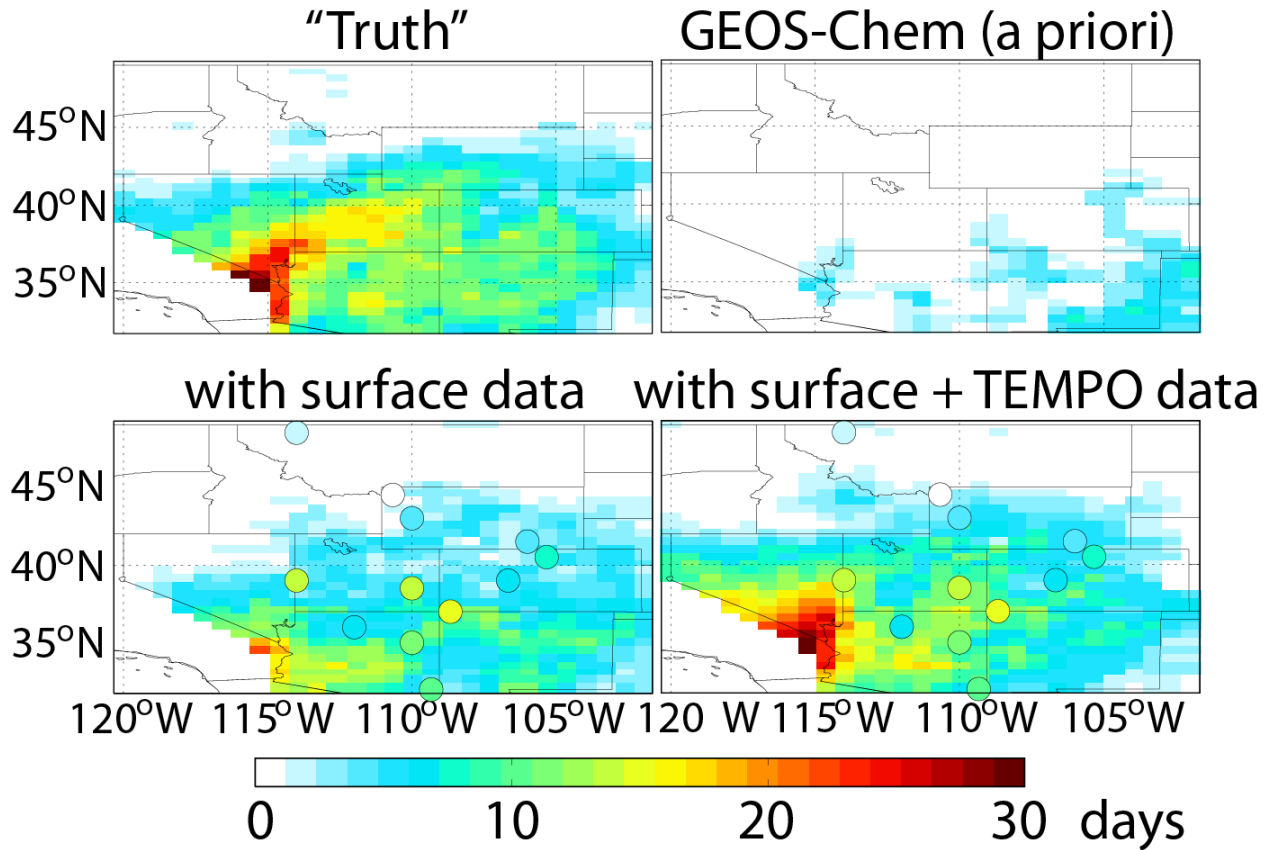
440 **Figure 3:** Error correlation length scales for the GEOS-Chem model simulation of tropospheric
441 ozone in the US Intermountain West. The error correlations are relative to actual CASTNet and
442 ozonesonde observations (in black) and relative to the GFDL AM3 model sampled in the
443 Intermountain West region (in red). Statistics are computed for April-June 2010. The left panel
444 shows the correlation coefficient (R) of the model error between pairs of CASTNet sites, plotted
445 against the distance between sites. Values are for the 12 CASTNet sites in the Intermountain
446 West (Figure 1). The right panel shows the correlation coefficient of the model error between
447 pairs of vertical levels (up to 8 km altitude) for ozonesonde measurements from the IONS-2010
448 campaign in California [Cooper et al. 2011], plotted against distance between levels.
449 Exponential fits to the data are shown inset, where d and z are horizontal and vertical distances in
450 km.



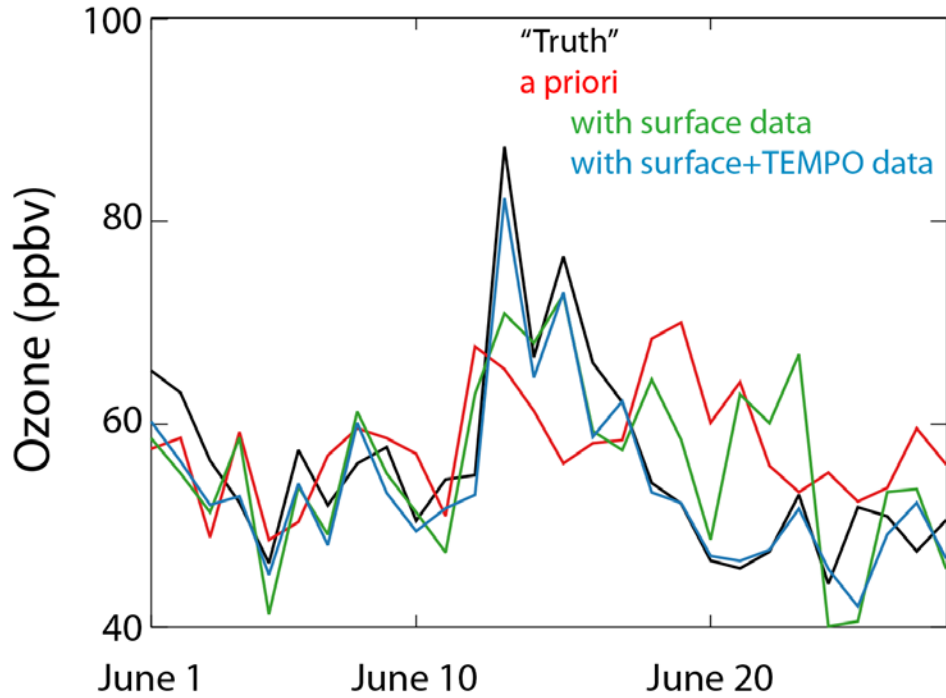
451

452 **Figure 4:** Improved monitoring of surface ozone across the Intermountain West from
 453 assimilation of synthetic CASTNet (surface) and TEMPO (geostationary satellite) observations.
 454 The figure shows scatterplots of simulated (GEOS-Chem) vs. “truth” (GFDL AM3) daily
 455 maximum 8-h (MDA8) surface ozone for April-June 2010 for all $1/2^\circ \times 2/3^\circ$ grid squares in the
 456 region (Figure 1) and for individual days. Results are for GEOS-Chem without data assimilation
 457 (top), with assimilation of CASTnet synthetic surface data (middle), and with additional
 458 assimilation of TEMPO and LEO synthetic satellite data (bottom). Comparison statistics are
 459 inset. Also shown are the reduced-major-axis (RMA) regression line and the 1:1 line.

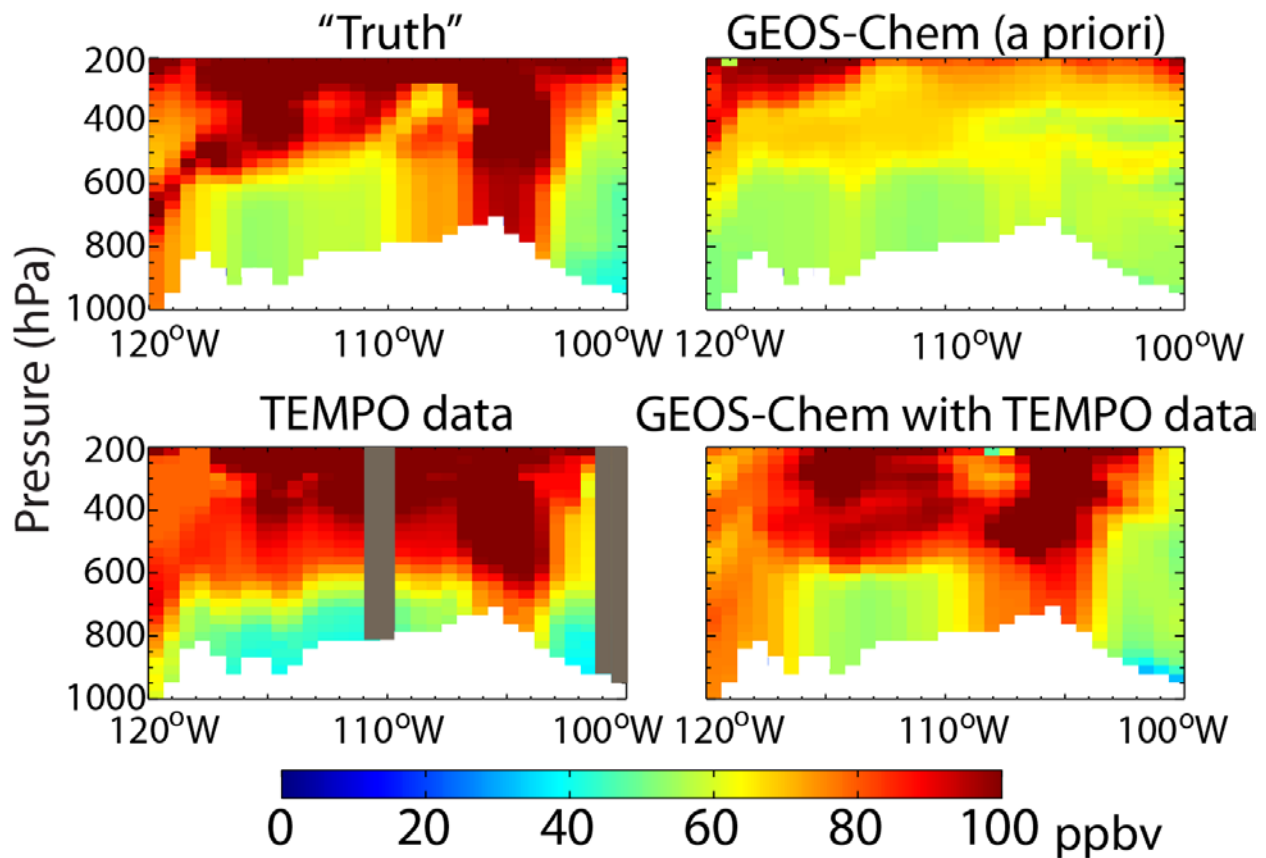
Number of days with MDA8 ozone > 70 ppbv



461 **Figure 5:** Improved detection of high-ozone events in the Intermountain West by data
462 assimilation. The figure shows the number of events (daily maximum 8-h ozone > 70 ppbv) in
463 April-June 2010 on the GEOS-Chem grid. The “truth” defined by the GFDL AM3 model (top
464 left panel) is compared to GEOS-Chem simulations without data assimilation (top right), with
465 assimilation of synthetic CASTNet surface data (bottom left), and with additional assimilation of
466 synthetic TEMPO and LEO satellite data (bottom right). Locations of CASTNet surface sites
467 used for assimilation with their “true” values are overlain in the bottom panels.



468
 469 **Figure 6:** Detection of an exceptional ozone event by TEMPO. The Figure shows the June 2010
 470 time series of daily maximum 8-h (MDA8) ozone concentrations at a location in northern New
 471 Mexico (107°W, 36°N) featuring a major stratospheric intrusion on June 13 in the GFDL AM3
 472 model taken as the “truth” (black line). The ability to capture this event is examined for the
 473 GEOS-Chem model without data assimilation (a priori, red line) and with assimilation of surface
 474 measurements only (green line) and satellite measurements added (blue line).



475 **Figure 7:** Longitude-altitude cross-section of ozone concentrations (36°N, 2100 MT on June 13,
 476 2010) associated with the stratospheric intrusion of Figure 6. The “true” state from the GFDL
 477 AM3 model (top left) is compared to the GEOS-Chem model without data assimilation (top
 478 right) and with assimilation of surface and satellite data (bottom right). The bottom left panel
 479 shows synthetic TEMPO observations of the “true” state (gray regions indicate cloudy scenes)
 480 without data assimilation. Orange and red values indicate ozone levels that would lead to
 481 exceedances of the current National Ambient Air Quality Standard (NAAQS) of 75 ppbv. Local
 482 topography is shown in white.
 483
 484

485 **References:**

486 Arnold, C. and Dey, C., 1986. Observing-systems simulation experiments - past, present, and
 487 future. *Bulletin of the American Meteorological Society* 67, 687-695.

488 August, T., Klaes, D., Schluessel, P., Hultberg, T., Crapeau, M., Arriaga, A., O'Carroll, A.,
 489 Coppens, D., Munro, R., Calbet, X., 2012. IASI on metop-A: Operational level 2
 490 retrievals after five years in orbit. *Journal of Quantitative Spectroscopy & Radiative*
 491 *Transfer* 113, 1340-1371.

- 492 Bak, J., Kim, J.H., Liu, X., Chance, K., Kim, J., 2013. Evaluation of ozone profile and
493 tropospheric ozone retrievals from GEMS and OMI spectra. *Atmospheric Measurement*
494 *Techniques* 6, 239-249.
- 495 Bey, I., Jacob, D., Yantosca, R., Logan, J., Field, B., Fiore, A., Li, Q., Liu, H., Mickley, L.,
496 Schultz, M., 2001. Global modeling of tropospheric chemistry with assimilated
497 meteorology: Model description and evaluation. *Journal of Geophysical Research-*
498 *Atmospheres* 106, 23073-23095.
- 499 Brodin, M., Helmig, D., Oltmans, S., 2010. Seasonal ozone behavior along an elevation gradient
500 in the colorado front range mountains. *Atmospheric Environment* 44, 5305-5315.
- 501 Chance, K., Lui, X., Suleiman, R.M., Flittner, D.E., Janz, S.J., 2012. Tropospheric Emissions:
502 Monitoring of Pollution (TEMPO). Abstract A31B-0020 presented at the 2012 AGU Fall
503 Meeting.
- 504 Chance, K., Burrows, J., Perner, D., Schneider, W., 1997. Satellite measurements of atmospheric
505 ozone profiles, including tropospheric ozone, from ultraviolet/visible measurements in
506 the nadir geometry: A potential method to retrieve tropospheric ozone. *Journal of*
507 *Quantitative Spectroscopy & Radiative Transfer* 57, 467-476.
- 508 Claeysman, M., Attie, J-L., Peuch, V-H., El Amraoui, L., Lahoz, W.A., Josse, B., Joly, M., Barre,
509 J., Ricaud, P., Massart, S., Piacentini, A., von Clarmann, T., Hopfner, M., Orphal, J.,
510 Flaud, J.M., Edwards, D.P., 2011. A thermal infrared instrument onboard a geostationary
511 platform for CO and O-3 measurements in the lowermost troposphere: Observing System
512 Simulation Experiments (OSSE). *Atm. Meas. Tech.*, 4, 1637-1661.
- 513 Clerbaux, C., Boynard, A., Clarisse, L., George, M., Hadji-Lazaro, J., Herbin, H., Hurtmans, D.,
514 Pommier, M., Razavi, A., Turquety, S., Wespes, C., Coheur, P.-., 2009. Monitoring of
515 atmospheric composition using the thermal infrared IASI/MetOp sounder. *Atmospheric*
516 *Chemistry and Physics* 9, 6041-6054.
- 517 Cooper, O.R., Oltmans, S.J., Johnson, B.J., Brioude, J., Angevine, W., Trainer, M., Parrish,
518 D.D., Ryerson, T.R., Pollack, I., Cullis, P.D., Ives, M.A., Tarasick, D.W., Al-Saadi, J.,
519 Stajner, I., 2011. Measurement of western US baseline ozone from the surface to the
520 tropopause and assessment of downwind impact regions. *Journal of Geophysical*
521 *Research-Atmospheres* 116, D00V03.
- 522 Cooper, O.R., Gao, R., Tarasick, D., Leblanc, T., Sweeney, C., 2012. Long-term ozone trends at
523 rural ozone monitoring sites across the United States, 1990-2010. *Journal of Geophysical*
524 *Research-Atmospheres* 117, D22307.
- 525 Edwards, D.P., Arellano, A.F., Jr., Deeter, M.N., 2009. A satellite observation system simulation
526 experiment for carbon monoxide in the lowermost troposphere. *Journal of Geophysical*
527 *Research-Atmospheres* 114, D14304.

- 528 Emery, C., Jung, J., Downey, N., Johnson, J., Jimenez, M., Yarvwood, G., Morris, R., 2012.
529 Regional and global modeling estimates of policy relevant background ozone over the
530 United States. *Atmospheric Environment* 47, 206-217.
- 531 Fiore, A., Jacob, D., Liu, H., Yantosca, R., Fairlie, T., Li, Q., 2003. Variability in surface ozone
532 background over the United States: Implications for air quality policy. *Journal of*
533 *Geophysical Research-Atmospheres* 108, 4787.
- 534 Fiore, A., Jacob, D., Bey, I., Yantosca, R., Field, B., Fusco, A., Wilkinson, J., 2002. Background
535 ozone over the United States in summer: Origin, trend, and contribution to pollution
536 episodes. *Journal of Geophysical Research-Atmospheres* 107, 4275.
- 537 Fishman, J., Iraci, L.T., Al-Saadi, J., Chance, K., Chavez, F., Chin, M., Coble, P., Davis, C.,
538 DiGiacomo, P.M., Edwards, D., Eldering, A., Goes, J., Herman, J., Hu, C., Jacob, D.J.,
539 Jordan, C., Kawa, S.R., Key, R., Liu, X., Lohrenz, S., Mannino, A., Natraj, V., Neil, D.,
540 Neu, J., Newchurch, M., Pickering, K., Salisbury, J., Sosik, H., Subramaniam, A.,
541 Tzortziou, M., Wang, J., Wang, M., 2012. The united states' next generation of
542 atmospheric composition and coastal ecosystem measurements NASA's geostationary
543 coastal and air pollution events (GEO-CAPE) mission. *Bulletin of the American*
544 *Meteorological Society* 93, 1547-+.
- 545 Fu, D., Worden, J.R., Liu, X., Kulawik, S.S., Bowman, K.W., Natraj, V., 2013. Characterization
546 of ozone profiles derived from aura TES and OMI radiances. *Atmospheric Chemistry and*
547 *Physics* 13, 3445-3462.
- 548 Ingmann, P., Veihelmann, B., Langen, J., Lamarre, D., Stark, H., Courreges-Lacoste, G.B., 2012.
549 Requirements for the GMES atmosphere service and ESA's implementation concept:
550 Sentinels-4/-5 and-5p. *Remote Sensing of Environment* 120, 58-69.
- 551 Jaffe, D., 2011. Relationship between surface and free tropospheric ozone in the western U.S.
552 *Environmental science & technology* 45, 432-438.
- 553 Jaffe, D.A. and Wigder, N.L., 2012. Ozone production from wildfires: A critical review.
554 *Atmospheric Environment* 51, 1-10.
- 555 Kaynak, B., Hu, Y., Martin, R.V., Russell, A.G., Choi, Y., Wang, Y., 2008. The effect of
556 lightning NO_x production on surface ozone in the continental united states. *Atmospheric*
557 *Chemistry and Physics* 8, 5151-5159.
- 558 Khattatov, B., Lamarque, J., Lyjak, L., Menard, R., Levelt, P., Tie, X., Brasseur, G., Gille, J.,
559 2000. Assimilation of satellite observations of long-lived chemical species in global
560 chemistry transport models. *Journal of Geophysical Research-Atmospheres* 105, 29135-
561 29144.

- 562 Kim, J., 2012. GEMS (Geostationary Environment Monitoring Spectrometer) onboard the
563 GeoKOMPSAT to monitor air quality in high temporal and spatial resolution over Asia-
564 Pacific region. Abstract EGU2012-4051 presented at the 2012 EGU General Assembly.
- 565 Lahoz, W.A., Peuch, V.-H., Orphal, J., Attie, J.-L., Chance, K., Liu, X., Edwards, D., Elbern, H.,
566 Flaud, J.-M., Claeys, M., El Amraoui, L., 2012. Monitoring air quality from space: the
567 case for the geostationary platform. *Bulletin of the American Meteorological Society* 11,
568 221-233.
- 569 Langford, A.O., Aikin, K.C., Eubank, C.S., Williams, E.J., 2009. Stratospheric contribution to
570 high surface ozone in Colorado during springtime. *Geophysical Research Letters* 36,
571 L12801.
- 572 Lefohn, A., Oltmans, S., Dann, T., Singh, H., 2001. Present-day variability of background ozone
573 in the lower troposphere. *Journal of Geophysical Research-Atmospheres* 106, 9945-9958.
- 574 Lin, M., Fiore, A.M., Cooper, O.R., Horowitz, L.W., Langford, A.O., Levy, Hiram, II, Johnson,
575 B.J., Naik, V., Oltmans, S.J., Senff, C.J., 2012. Springtime high surface ozone events
576 over the western United States: Quantifying the role of stratospheric intrusions. *Journal*
577 *of Geophysical Research-Atmospheres* 117, D00V22.
- 578 Lin, M., Fiore, A.M., Horowitz, L.W., Cooper, O.R., Naik, V., Holloway, J., Johnson, B.J.,
579 Middlebrook, A.M., Oltmans, S.J., Pollack, I.B., Ryerson, T.B., Warner, J.X.,
580 Wiedinmyer, C., Wilson, J., Wyman, B., 2012. Transport of asian ozone pollution into
581 surface air over the western United States in spring. *Journal of Geophysical Research-*
582 *Atmospheres* 117, D00V07.
- 583 Liu, X., Sioris, C., Chance, K., Kurosu, T., Newchurch, M., Martin, R., Palmer, P., 2005.
584 Mapping tropospheric ozone profiles from an airborne ultraviolet-visible spectrometer.
585 *Applied Optics* 44, 3312-3319.
- 586 Lord, S.J., Kalnay E., Daley R., Emmitt G.D., Atlas R., 1997. Using OSSEs in the design of future g
587 eneration integrated observing systems. Preprints, 1st Symposium on Integrated Observing
588 Systems, Long Beach, CA, AMS, 45-47.
- 589 Mueller, S.F. and Mallard, J.W., 2011. Contributions of natural emissions to ozone and PM_{2.5} as
590 simulated by the community multiscale air quality (CMAQ) model. *Environmental*
591 *science & technology* 45, 4817-4823.
- 592 Natraj, V., Liu, X., Kulawik, S., Chance, K., Chatfield, R., Edwards, D.P., Eldering, A., Francis,
593 G., Kurosu, T., Pickering, K., Spurr, R., Worden, H., 2011. Multi-spectral sensitivity
594 studies for the retrieval of tropospheric and lowermost tropospheric ozone from simulated
595 clear-sky GEO-CAPE measurements. *Atmospheric Environment* 45, 7151-7165.
- 596 Parrington, M., Jones, D.B.A., Bowman, K.W., Horowitz, L.W., Thompson, A.M., Tarasick,
597 D.W., Witte, J.C., 2008. Estimating the summertime tropospheric ozone distribution over

598 North America through assimilation of observations from the tropospheric emission
599 spectrometer. *Journal of Geophysical Research-Atmospheres* 113, D18307.

600 Parrish, D.D., Aiken, K.C., Oltmans, S.J., Johnson, B.J., Ives, M., Sweeny, C., 2010. Impact of
601 transported background ozone inflow on summertime air quality in a California ozone
602 exceedances area. *Atmospheric Chemistry and Physics* 10, 10093-10109.

603 Reid, N., Yap, D., Bloxam, R., 2008. The potential role of background ozone on current and
604 emerging air issues: An overview. *Air Quality Atmosphere and Health* 1, 19-29.

605 Rodgers, C.D., 2000. *Inverse Methods for Atmospheric Sounding*. World Scientific, River Edge,
606 New Jersey.

607 Selitto, P., Dufour, G., Eremenko, M., Cuesta, J., Foret, G., Gaubert, B., Beekmann, M., Peuch,
608 V.-H., Flaud, J.-M., 2014. Monitoring the lowermost tropospheric ozone with thermal
609 infrared observations from a geostationary platform: performance analyses for a future
610 dedicated instrument. *Atmospheric Measurement Techniques* 7, 391-407.

611 Selitto, P., Del Frate, F., Solimini, D., Casadio, S., 2012. Tropospheric ozone column retrieval
612 from ESA-Envisat SCIAMACHY nadir UV/VIS radiance measurements by means of a
613 neural network algorithm. *IEEE Transactions on Geosciences and Remote Sensing* 50,
614 998-1011.

615 Selitto, P., Di Noia, A., Del Frate, F., Burini, A., Casadio, S., Solimini, D., 2012. On the role of
616 visible radiation in ozone profile retrieval from nadir UV/VIS satellite measurements: An
617 experiment with neural network algorithms inverting SCIAMACHY data. *Journal of*
618 *Quantitative Spectroscopy and Radiative Transfer* 113, 1429-1436.

619 Singh, H.B., Cai, C., Kaduwela, A., Weinheimer, A., Wisthaler, A., 2012. Interactions of fire
620 emissions and urban pollution over California: Ozone formation and air quality
621 simulations. *Atmospheric Environment* 56, 45-51.

622 Timmermans, R.M.A., Segers, A.J., Builtjes, P., Vautard, R., Siddans, R., Elbern, H., Tjemkes,
623 S., Schaap, M., 2009. The added value of a proposed satellite imager for ground level
624 particulate matter analyses and forecasts. *IEEE J. Sel. Top. Appl.*, 2, 271-283.

625 United States Environmental Protection Agency, 2010. Clean air status and trends network
626 second quarter 2010 quality assurance report.

627 United States Environmental Protection Agency, 2012. *Welfare Risk and Exposure Assessment*
628 *for Ozone*.

629 United States Environmental Protection Agency, 2013. *Interim Guidance to Implement*
630 *Requirements for the Treatment of Air Quality Monitoring Data Influenced by*
631 *Exceptional Events*.

- 632 Worden, H.M., Deeter, M.N., Frankenberg, C., George, M., Nichitiu, F., Worden, J., Aben, I.,
633 Bowman, K.W., Clerbaux, C., Coheur, P.F., de Laat, A.T.J., Detweiler, R., Drummond,
634 J.R., Edwards, D.P., Gille, J.C., Hurtmans, D., Luo, M., Martinez-Alonso, S., Massie, S.,
635 Pfister, G., Warner, J.X., 2013. Decadal record of satellite carbon monoxide observations.
636 *Atmospheric Chemistry and Physics* 13, 837-850.
- 637 Yates, E.L., Iraci, L.T., Pierce, R.B., Johnson, M.S., Reddy, P.J., Tadic, J.M., Loewenstein, M.,
638 Gore, W., 2013. Airborne observations and modeling of springtime stratosphere-to-
639 troposphere transport over California. *Atmos. Chem. Phys. Discuss.* 13,
- 640 Zhang, L., Jacob, D.J., Boersma, K.F., Jaffe, D.A., Olson, J.R., Bowman, K.W., Worden, J.R.,
641 Thompson, A.M., Avery, M.A., Cohen, R.C., Dibb, J.E., Flock, F.M., Fuelberg, H.E.,
642 Huey, L.G., McMillan, W.W., Singh, H.B., Weinheimer, A.J., 2008. Transpacific
643 transport of ozone pollution and the effect of recent Asian emission increases on air
644 quality in North America: An integrated analysis using satellite, aircraft, ozonesonde, and
645 surface observations. *Atmospheric Chemistry and Physics* 8, 6117-6136.
- 646 Zhang, L., Jacob, D.J., Liu, X., Logan, J.A., Chance, K., Eldering, A., Bojkov, B.R., 2010.
647 Intercomparison methods for satellite measurements of atmospheric composition:
648 Application to tropospheric ozone from TES and OMI. *Atmospheric Chemistry and*
649 *Physics* 10, 4725-4739.
- 650 Zhang, L., Jacob, D.J., Downey, N.V., Wood, D.A., Blewitt, D., Carouge, C.C., van Donkelaar,
651 A., Jones, D.B.A., Murray, L.T., Wang, Y., 2011. Improved estimate of the policy-
652 relevant background ozone in the United States using the GEOS-chem global model with
653 1/2 degrees x 2/3 degrees horizontal resolution over North America. *Atmospheric*
654 *Environment* 45, 6769-6776.
- 655 Zoogman, P., Jacob, D.J., Chance, K., Worden, H.M., Edwards, D.P., Zhang, L., 2014. Improved
656 monitoring of surface ozone air quality by joint assimilation of geostationary satellite
657 observations of ozone and CO. *Atmospheric Environment* 84, 254-261.
- 658 Zoogman, P., Jacob, D.J., Chance, K., Zhang, L., Le Sager, P., Fiore, A.M., Eldering, A., Liu,
659 X., Natraj, V., Kulawik, S.S., 2011. Ozone air quality measurement requirements for a
660 geostationary satellite mission. *Atmospheric Environment* 45, 7143-7150.